

C–O–H–N fluid inclusions associated with gold–stibnite mineralization in low-grade metamorphic rocks, Mari Rosa mine, Cáceres, Spain

L. ORTEGA,* E. VINDEL AND C. BENY†

* Dpto. Cristalografía y Mineralogía, Universidad Complutense, 28040 Madrid, Spain

† GIS-BRGM CNRS, 45071 Orléans Cedex-2, France

Abstract

The Mari Rosa mine lies within a low-grade Precambrian alternating series of black shales and metagreywackes in the Spanish Hercynian massif. There are two generations of mineralized veins: V2, gold–(stibnite)-bearing quartz veins, parallel to the main cleavage, and V3, stibnite-bearing quartz veins which postdate the main deformation event.

Four main types of inclusions have been identified. Type I, II and IV are aqueous–carbonaceous inclusions, with variable degrees of filling, while type III are non-aqueous and typically single-phase at room temperature. Except for type I (absent in V3), similar inclusions have been observed in both V2 and V3 veins. Gas compositions are always characterised by CH₄–N₂–CO₂ assemblages, ranging from CO₂-rich mixtures in the earliest inclusions (type I), to N₂-rich mixtures in the latest inclusions (type IV).

Gold precipitation in V2 veins can be related to type I inclusions at $T > 380^\circ\text{C}$ ($T_H = 300\text{--}380^\circ\text{C}$). A subsequent drop in X_{CO_2} and cooling are recorded in type II and III inclusions, interpreted to be the result of unmixing of a previously homogeneous fluid derived from type I. This boiling would provoke the precipitation of stibnite at 300°C and 1 kbar. The type IV inclusions, which are the richest in H₂O, represent a late fluid circulation at lower temperatures ($T_H = 190\text{--}280^\circ\text{C}$).

KEYWORDS: fluid inclusions, gold, stibnite, Cáceres, Spain.

Introduction

IN the Hercynian sector of the Iberian peninsula there are several occurrences of Sb–Au mineralization distributed along a wide zone, defining the so-called ‘quartz–gold–antimoniferous belt’ (Gumiel *et al.*, 1976; Gumiel and Arribas, 1987) which parallels the NW–SE Hercynian structures in central-western Spain and Portugal. This paper presents a fluid-inclusion study of one of these mineralizations, at the Mari Rosa mine.

Geological setting

The Mari Rosa Sb–Au deposit is located on the southern border of the Central Iberian Zone, Iberian Hercynian massif (Fig. 1), and was previously studied by Gumiel (1983). The host rocks belong to the ‘Complejo Esquisto Grauváquico’ (Schist–Greywacke complex), a thick series of detrital sediments of Upper Precambrian age.

Within the area, this series is made up of an alternating sequence of phyllites, greywackes and black shales, with a chlorite–albite–white-mica assemblage consistent with lower greenschist facies metamorphism. The Nisa–Albuquerque batholith, made up of granites and granodiorites, outcropping 15 km away from the mine, and develops a contact metamorphism aureole of 1 km wide (Martín Herrero and Bascones, 1979). The structure of the area is mainly due to the Hercynian Orogeny, and involves two phases of deformation. The first and main phase produced chevron folds and a vertical NW–SE slaty cleavage (S1); the second phase was less intense and caused local crenulation and kink banding (Quesada *et al.*, 1987).

Based upon the relationships with the main Hercynian structures, three generations of veins have been recognized in the sector of Mari Rosa mine, as follows:

A. V1 veins: folded pyrite-bearing quartz veinlets

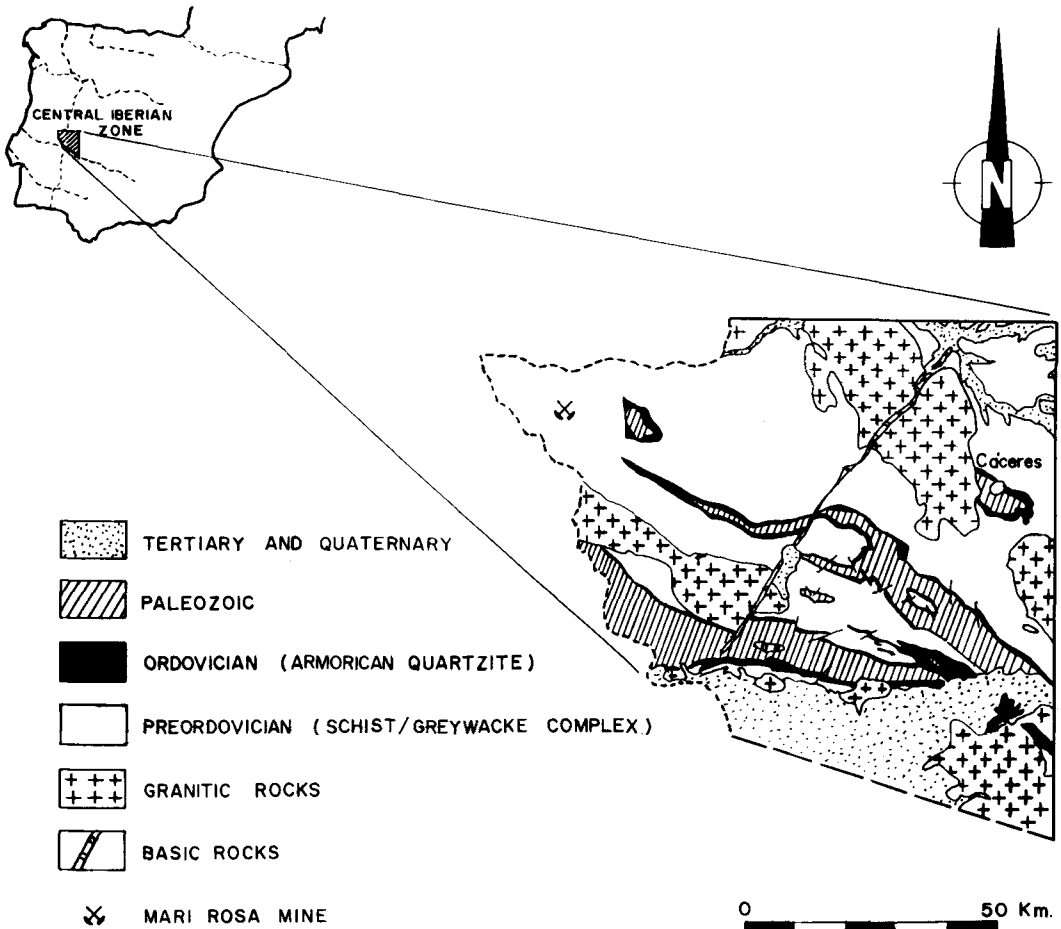


Fig. 1. Locality and geological map of the study area.

that represent veining previous to regional metamorphism.

B. V2 veins: pyrrhotite-pyrite-stibnite-arsenopyrite-gold-carbonate-bearing quartz veins, parallel to the main Hercynian cleavage. They show pinch and swell structures, up to 10 cm thick. Native gold occurs, filling cracks as well as inclusions in quartz and in arsenopyrite (Gumiel, 1983).

C. V3 veins: stibnite-bearing quartz veins cross-cutting the main Hercynian cleavage and V2 type veins. They have lensoid morphology with stibnite occurring in pods.

Wall rock alteration is generally weak and restricted to a narrow zone adjacent to the veins. Intermediate argillic alteration occurs mainly in V3 veins and chloritization has been observed in relation to V2 veins. Close to these veins, black

shales are invaded by minor carbonates and sulphides related to the V2 mineralization.

Sampling and analytical techniques

Although the highest gold grades are reported from the -9 m level of the mine, the workings are inaccessible at present due to flooding. Therefore, quartz samples were collected from V1, V2 and V3 veins from the main level of the mine (0 m), where stibnite is the more abundant ore mineral. Microthermometric analyses were carried out using a Chaixmecca stage (Poty *et al.*, 1976). The stage was calibrated at low temperatures with a CO₂ natural fluid inclusion at the triple point (-55.6 °C) and the melting point of toluene (-95 °C).

Compositions of the non-aqueous part of

TABLE 1. Explanations of the symbols used in text and figures.

Cl:	clathrate.
d:	bulk density of the inclusion (g.cm^{-3})
dv:	density of the nonaqueous part (g.cm^{-3})
Dfc:	degree of filling of the nonaqueous part of the inclusion.
T_{H1} :	total homogenization temperature for H_2O -bearing inclusions; (L): to the liquid.
T_h :	homogenization temperature of the non-aqueous part.
$T_h \text{ CH}_4\text{-N}_2$:	homogenization temperature of the non-aqueous part ($^\circ\text{C}$) for $T_h < T_m \text{ CO}_2$; it is assumed that all of the CO_2 is partitioned in the solid phase at this T_h .
$T_h \text{ CO}_2$:	homogenization temperature of the non-aqueous part ($^\circ\text{C}$) for $T_h > T_m \text{ CO}_2$; (L): to the liquid, (V): to the vapour, (C): critical.
$T_m \text{ Cl}$:	melting temperature of clathrate ($^\circ\text{C}$).
$T_m \text{ ice}$:	melting temperature of ice ($^\circ\text{C}$).
\bar{V} :	molar volume ($\text{cm}^3.\text{mol}^{-1}$).
\bar{V}_v :	molar volume of the nonaqueous part of the fluid (above T_h) ($\text{cm}^3.\text{mol}^{-1}$).
\bar{V}_i :	bulk molar volume ($\text{cm}^3.\text{mol}^{-1}$).
V1::	first generation of quartz veins.
V2:	second generation of quartz veins.
V3:	third generation of quartz veins.
X:	composition (molar fraction).
X_i :	molar fraction of a given component (CH_4 , CO_2 , N_2).
%i:	mole % of a given component (CH_4 , CO_2 , N_2).

individual inclusions were measured using a MOLE Raman microprobe (Dhamelincoourt *et al.*, 1979; Touray *et al.*, 1985). The Raman microprobe used was a type U1000 double monochromator (manufactured by JOBIN-YVON) with a RCA 31034 photomultiplier (U.S.A.) as detector. The monochromatic exciting light at 514.5 nm was produced by an ionised argon laser of INNOVA 90-5 type (COHERENT, U.S.A.).

Fluid inclusion study

Although attempts were made to study fluid inclusions in quartz from all three veins, those present in the V1 veins were generally too small, and most of them exhibited characteristic leakage and necking-down phenomena. Therefore, thermometric data from V1 samples were unattainable.

Based on microscopic, microthermometric and Raman spectroscopic features, four main types (Fig. 2) of fluid inclusions have been distinguished in the remaining V2 and V3 veins. Type I are present only in samples from V2 veins, and type II, III and IV are found both in V2 and V3 veins.

Type I inclusions occur systematically in clear parts of quartz crystals (Fig. 3a) and are not very abundant. The inclusions are two-phase at room

temperature with a nonaqueous bubble occupying 40–60% of the volume of the cavity. The size ranges between 5–20 μm . Melting temperatures of the CO_2 range from -73.5 to -61.0 and $T_h \text{ CO}_2$ occurred between -45 to -19 $^\circ\text{C}$, both reflecting strong contamination of CO_2 by CH_4 and/or N_2 (Swanenberg, 1979; Kreulen and Schuiling, 1982). This is confirmed by Raman analysis (Table 2), which reveals that even if CO_2 is the main component, important quantities of CH_4 and N_2 are present in the non-aqueous part of the inclusions. Homogenization of CO_2 is always to the vapour phase. However, sublimation from solid to vapour at -66.8 $^\circ\text{C}$ has been observed in one fluid inclusion. Because of the volume of the bubble and clathration, only two $T_m \text{ ice}$ values have been measured at -8.4 and -3.8 $^\circ\text{C}$. Clathrates melt between $+9.5$ and $+14.5$ $^\circ\text{C}$. Total homogenization is sometimes impossible to measure, as decrepitation occurs, between $+230$ and $+310$ $^\circ\text{C}$, before homogenization. This is caused by the high internal pressures developed in inclusions containing CO_2 and/or CH_4 (Roedder, 1984). Homogenization measurements are between $+275$ and $+377$ $^\circ\text{C}$, into L, rarely C.

Type II inclusions are, together with type III inclusions, the most abundant in all samples and usually have a regular shape. They are biphasic with a rather constant degree of filling by the vapour phase of around 15–25%. The size ranges from 10 to 25 μm . Sometimes, trapped solids have been observed. On cooling, a solid phase appears in the bubble below -35 $^\circ\text{C}$, simultaneously with the freezing of the aqueous part (Fig. 3C). The freezing runs were usually carried out, down to -170 $^\circ\text{C}$. However, no further phase transitions were observed, in spite of Raman analyses of the vapour phase which indicates mixtures of $\text{CO}_2\text{-CH}_4\text{-N}_2$ (poorer in CO_2 than type I inclusions). The reason for this might be that the remaining fluid after clathration is not dense enough to nucleate another L or V phase in the bubble. Another possibility is that the heterogenization/homogenization processes are not optically distinguishable by the small size of the bubble. On warming, the solid phase nucleated on cooling melts typically a few degrees below melting of ice, recorded from -6 to -2 $^\circ\text{C}$. Between $+5$ and $+8$ $^\circ\text{C}$, a sudden movement of the bubble in the inclusion is indicative of final melting of clathrate. If an inclusion is cooled again before this movement, the bubble appears distorted and solid black grains nucleate in the aqueous part during the subsequent warming which confirm the presence of a gas hydrate. The precise temperature of dissociation of the clath-

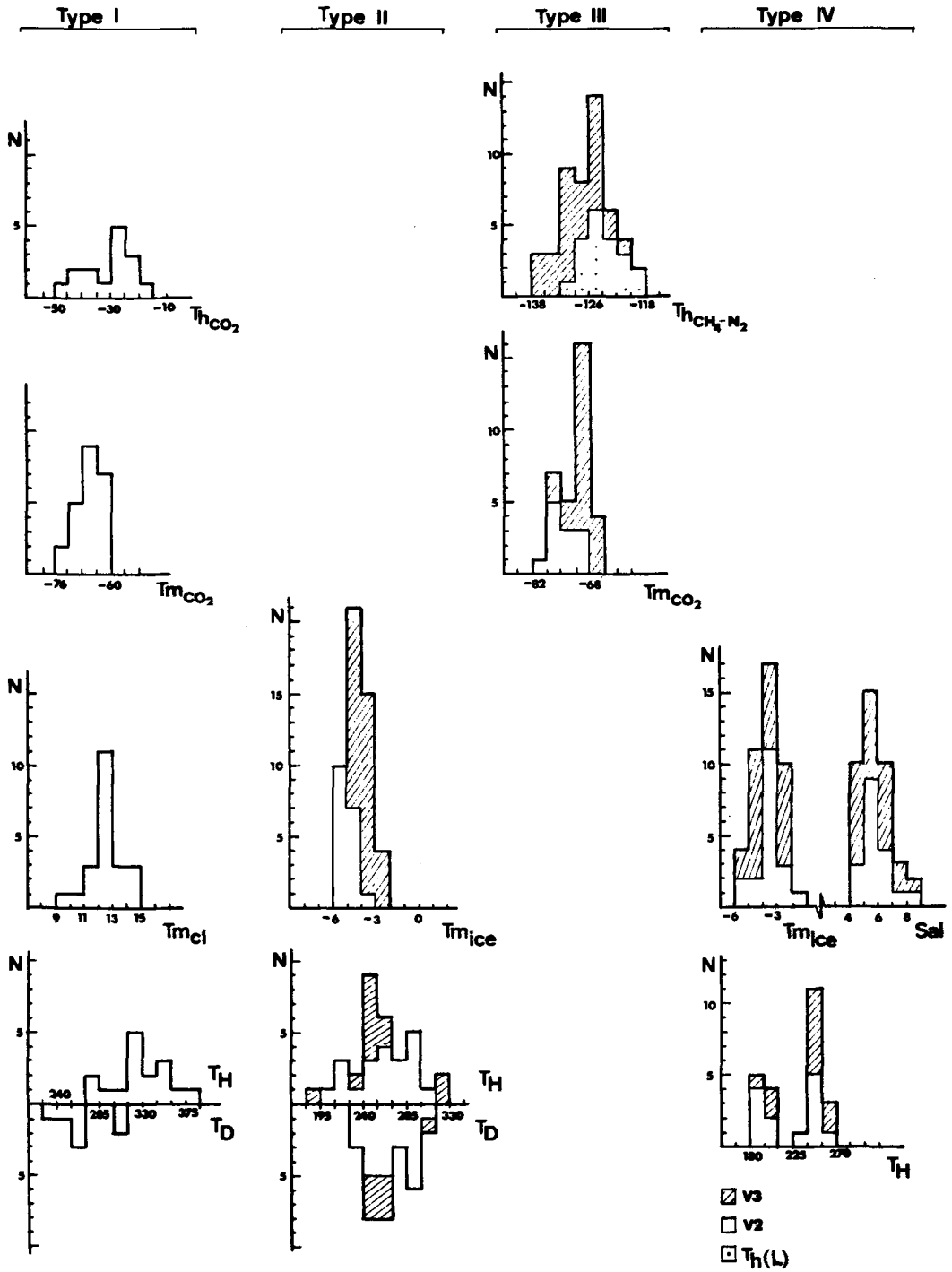


FIG. 2. Histograms of the microthermometric measurements (°C) on the four types of fluid inclusions.

TABLE 2. Microthermometric (T_m CO₂ and T_h CO₂) and Raman results for the nonaqueous part of representative inclusions from Mari Rosa V2 and V3 quartz veins. Raman data are not available for V2 type IV inclusions because bubbles move during the spectroscopic analysis. T_h CO₂ means T_h CH₄-N₂ in type III. Phase transitions at low temperatures have not been seen in type II and IV inclusions. n.d.: not detected.

Type of inclusion and number of sample			Dfc	Microthermometry		Raman spectroscopy		
				T_m CO ₂	T_h CO ₂	%CH ₄	%N ₂	%CO ₂
I 	V2	2MR-1	0.6	-70.0	-27.6 (V)	34.7	14.0	51.2
		2MR-2	0.5	-68.7	-45.2 (V)	33.6	17.5	48.9*
		2MR-3	0.6	-73.5	-44.6 (V)	42.7	22.9	34.4
		2MR-89	0.4	-68.1	-35.6 (V)	29.3	9.6	61.1
II 	V2	2MR-45	0.25			23.4	42.9	33.7
		2MR-94	0.2			17.6	49.8	32.6
	V3	MR-138	0.2			15.6	47.9	36.5
		MR-139	0.15			10.6	49.9	39.5
		MR-140	0.25			5.7	58.4	35.9
		MR-141	0.25			12.1	46.8	41.1
		MR-142	0.3			9.3	51.8	38.9
		MR-144	0.2			11.3	59.8	28.9
III 	V2	2MR-46		-76.1	-124.8 (L)	26.3	56.8	16.9
		2MR-50		-76.2	-125.3 (L)	28.3	57.4	14.3
		2MR-116		-71.0	-120.4 (V)	21.7	57.4	20.8
		2MR-117		-71.5	-121.1 (V)	23.3	55.8	20.9
	V3	MR-66		-69.6	-128.4 (V)	18.3	60.9	20.8
		MR-70		-	-129.6 (V)	16.5	64.0	19.5
		MR-184		-70.9	-131.1 (V)	17.7	64.0	18.3
IV 	V3	MR-78	0.1			22.6	77.4	n.d.
		MR-182	0.05			23.9	76.1	n.d.

* Some amounts of carbon have been detected in this fluid inclusion.

rate was determined in a number of inclusions using a cyclic multiphasic cooling as defined by Collins (1979).

The solid phase which nucleated at -35°C within the bubble has been interpreted as a clathrate. It starts to melt at a given low temperature and becomes invisible when the pressure of ice on the bubble decreases close to ice melting point. However, it remains present in the inclusion until the recorded temperatures reach $+5$ to $+8^{\circ}\text{C}$. As an alternative, it has been also considered that this solid phase could be ice, nucleated from water vapour dissolved in the bubble. However, this seems less probable given the small quantities of water that can be contained in the carbonic phase (0.1 wt.% H₂O at 22.5°C in liquid CO₂; Stone, 1943, cited in Roedder, 1984). Nevertheless, a further investigation of this proposal should be made. Total homogenization at temperatures ranging from $+190$ to $+330^{\circ}\text{C}$, are always in the liquid phase. Decrepitation before homogenization took place in about 50% of the samples at temperatures between $+230$ and $+310^{\circ}\text{C}$. The size of the decrepitated inclusions was always larger than $15\ \mu\text{m}$.

Type III inclusions are very abundant,

especially in certain parts of the quartz samples. They have either ovoid or irregular shapes, and are up to $20\ \mu\text{m}$ in size. These fluid inclusions appear single-phase at room temperature and correspond to type S2 inclusions of van den Kerkhof (1988 a, b). At low temperatures (below -110°C) vapour and liquid coexist with grains of solid CO₂. Temperatures of homogenization range from -128 to -118°C in V2 veins (sometimes V, sometimes L) and from -138 to -121°C in V3 veins (always in vapour, but near critical). Phase transitions in this low-temperature region correspond to compositions in the system CH₄-N₂, subsequently confirmed by Raman spectroscopy (Table 2). Solid CO₂ sublimates at temperatures between -76.2 to -70.3°C in V2 veins and -77.2 to -66°C in V3 veins. Sublimation is characteristic of low molar volumes and high contents of N₂ and/or CH₄ (Burrus, 1981). Similar fluid inclusions, even though from high-grade metamorphic rocks, have been described by Swanenberg (1980), Kreulen and Schuiling (1982), and van den Kerkhof (1988b).

Type IV consist of small ($<10\ \mu\text{m}$) biphasic inclusions, with the vapour phase occupying up to

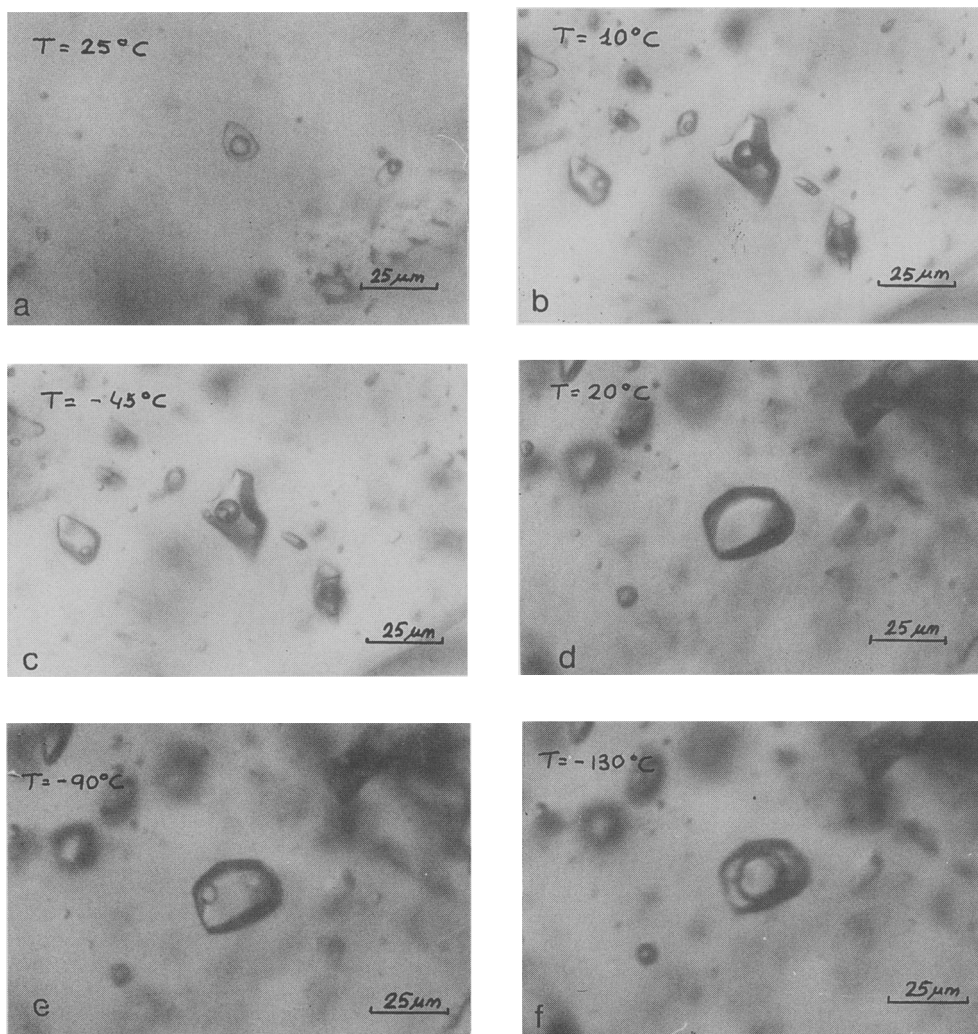


FIG. 3. Types of fluid inclusions in quartz veins: (a) isolated type I inclusion; (b, c) type II inclusion; two-phase at room temperature, a solid nucleated in the bubble below -35°C ; (d, e, f) type III inclusion, behaviour at low temperatures.

10 volume %. They are scarce. N_2 and minor CH_4 have been detected by Raman microprobe in the nonaqueous part of the inclusions. However, liquid/vapour transitions have not been observed at low temperatures, because of the small size of the vapour bubble and/or the low density of the fluid. Melting temperatures of ice are scattered between -5.2 and -1.5°C and hydrates have not been observed. On heating, homogenization to liquid takes place within the range $+188$ to $+266^{\circ}\text{C}$. Decrepitation before homogenization is not usual in this type of inclusion.

Mode of occurrence

The relative age of the different generations of inclusions, as well as their primary or secondary character, can be deduced from their occurrence in quartz veins. Criteria for primary/secondary origin are from Roedder (1976).

The oldest inclusions are type I, which are present only in V2 veins and, therefore, predate V3 veins and the main stibnite mineralizing event. They usually occur isolated in clear parts of quartz crystals and are early, probably primary inclusions.

A quartz crystal showing growth zonation has been observed in a sample from V3 veins (Fig. 4), and type II fluid inclusions have been recognized as primary inclusions in this sample. Furthermore, small grains of stibnite appear in these growth faces, showing a close relationship between type II inclusions and mineralization. In V2 samples they occur in clusters or as pseudo-secondary inclusions, in fractures visibly terminating within crystal. They are later than type I.

Type III inclusions occur aligned, as well as in clusters, within both type of veins. In the V3 zoned quartz sample, they are generally distributed in rough arrangements crossing the growth faces. However, in the same sample, they also appear in arrays which are subparallel and adjacent to primary type II inclusions trails, in growth directions. This occurrence can be indicative of a heterogeneous fluid (Roedder, 1976). Both types II and III inclusions are widely distributed in all samples and appear closely related. They are probably contemporaneous.

Type IV are secondary inclusions. They always occur in fractures and postdate all other types.

Compositional observations support the above chronological succession given that a progressive enrichment in N_2 in the vapour phase of the inclusions has been observed from type I to type IV, following the same succession (Fig. 5).

Discussion

Clathrate hydrates. Hydrates in the system $H_2O-CO_2-CH_4-N_2$ are solid solutions among CO_2 , CH_4 and N_2 clathrates (Hollister and Burrus, 1976). Taking CO_2 hydrate as a reference, the presence of other components raises the temperature of dissociation of the clathrate, typically up to $10^\circ C$ for pure CO_2 clathrate (Collins, 1979). Only N_2 (Hand *et al.*, 1974) and

$NaCl$ (Chen, 1972; Bozzo *et al.*, 1975) has a depressing effect. Hence, in mixed clathrates the presence of some components may be masking the presence of others, and their composition is not easy to estimate from microthermometric measurements alone.

In type I inclusions, clathrate melts within a narrower range between $+10$ to $+15^\circ C$. This clathrate is interpreted to be a CO_2-CH_4 hydrate, the two main volatile species present in the inclusions. Regarding the different partitioning of these two components between clathrate and fluid, contradictory data are recorded in the literature. Some authors (Unruh and Katz, 1949; Parrish and Prausnitz, 1972; Dubessy *et al.*, 1989) indicate that in mixtures with other, more volatile gases, CO_2 shows a preferential partitioning into a solid phase, i.e. clathrate. However, the opposite conclusions have been reached by Seitz *et al.* (1987). It is an important question to elucidate since the composition of the remaining non-aqueous fluid after clathration change from that recorded by Raman spectroscopy at room temperature. This is observed in type I inclusions, where the microthermometric results for $T_h CO_2$ in the presence of clathrate indicate that, at this point, the non-aqueous fluid is poorer in CO_2 than the same fluid after clathrate dissociation. Therefore, in this case, the clathrate must be a CO_2 -rich clathrate, which is in agreement with the first authors cited.

Clathrate in type II inclusions shows melting temperatures which could correspond to a CO_2 -hydrate. However, given the relative proportions of the non-aqueous compounds in these inclusions, an N_2 -rich clathrate would be more probable. In the absence of additional data, an estimate of the hydrate composition is not possible.

Salt content of the aqueous part. The presence of complex hydrates in type I and II inclusions

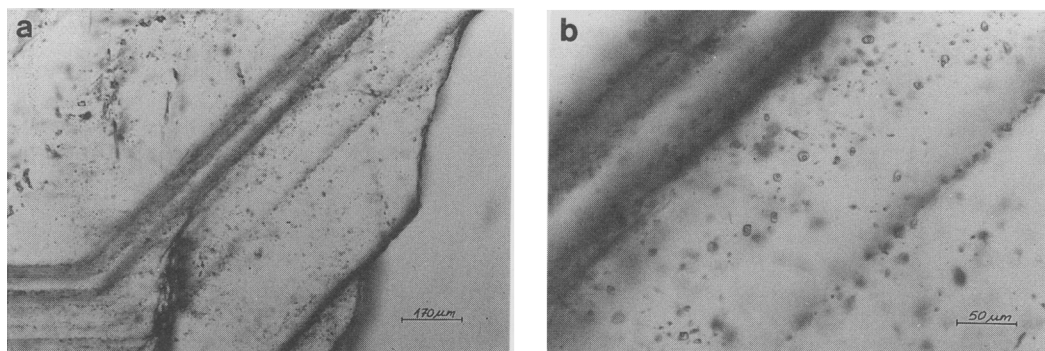


FIG. 4 (a, b). Growth zoning quartz with primary type II inclusions parallel to growth planes.

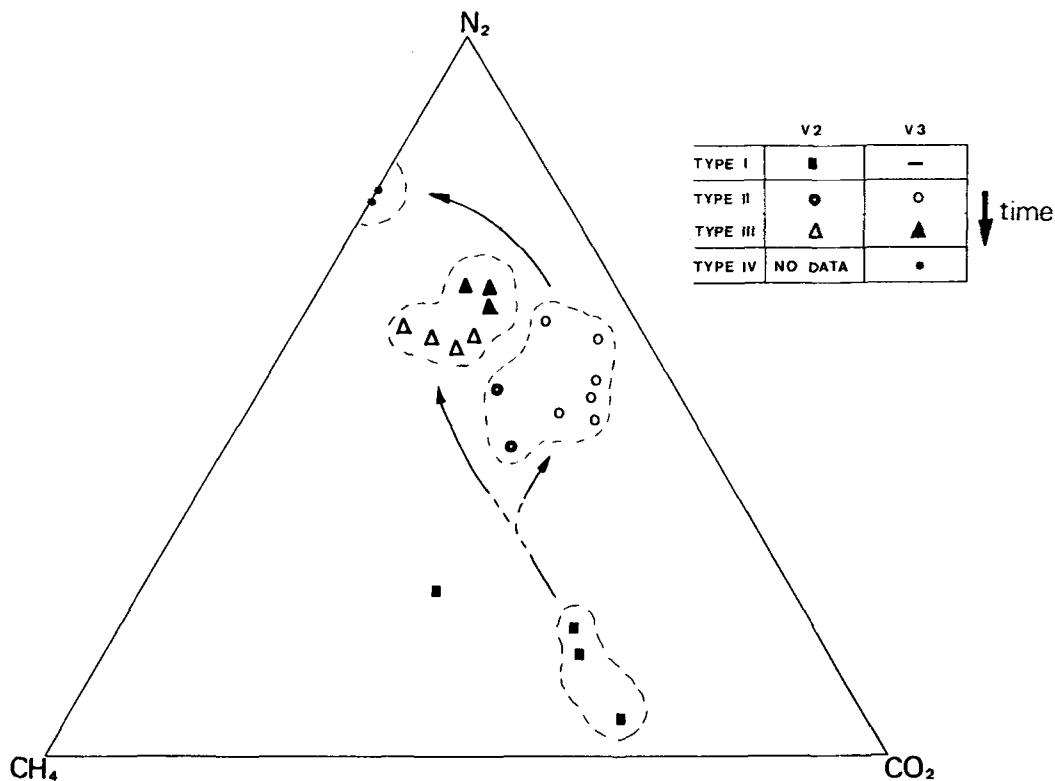


Fig. 5. Composition of the non-aqueous part (% mol) and evolution of fluid inclusions from the mineralized V2 and V3 quartz veins for the N_2 - CO_2 - CH_4 system.

prevents the derivation of the salinity data from both T_m ice and T_m Cl. Salt content in type IV ranges between 2.5 to 9% eq NaCl. These data have been determined from T_m ice, because clathrate formation has not been observed. Nevertheless, even if CH_4 hydrates are absent, the presence of CH_4 in aqueous inclusions will cause a depression of the freezing point of water and, hence, an increase in the apparent salinity because of the effect of the pressure on the ice-water equilibria (Hanor, 1980; Roedder, 1985). Therefore, the data given above can be higher rather than true values. No reference concerning the influence of N_2 on salinity estimates using microthermometry has been recorded in the literature.

Composition and molar volume data. Ten inclusions from V2 and eleven from V3 veins have been analysed by Raman spectroscopy. The results are recorded in Table 2. Most of the inclusions have intermediate compositions in the CO_2 - CH_4 - N_2 system. Experimental data on this ternary system pertaining to microthermometric analysis are not available. Therefore an approxi-

mation is made from published data on the CO_2 - N_2 , CO_2 - CH_4 and CH_4 - N_2 binary systems (van den Kerkhof, 1988b).

Type I fluid inclusions could be plotted within the system CO_2 - CH_4 taking N_2 as CH_4 , i.e. $X_{eq}CH_4 = XCH_4 + XN_2$ (Ramboz *et al.*, 1985). Such inclusions are characterized by T_m CO_2 and T_h CO_2 in the presence of a complex clathrate, preventing a quantitative interpretation of these measurements and the T_m Cl in terms of molar volume (\bar{V}). Nevertheless, given that homogenization of the CO_2 phase is into the vapour, and at very low temperatures, high molar volumes and low densities can be expected for the non-aqueous part of type I inclusions.

A point to take into account is the presence of carbon (less organized than graphite) in at least one of these inclusions (Table 2), detected by Raman spectroscopy. When carbon compounds are present in fluid inclusions, $\bar{V}X$ properties obtained from microthermometry and Raman spectroscopy can be rather different from the values of these parameters at trapping conditions (Dubessy, 1984). This is due to chemical re-

equilibration during cooling. Therefore, the composition obtained by spectroscopic analysis can be slightly different from the composition at the time of trapping.

Type II inclusions approximate to compositions in the $\text{CO}_2\text{-N}_2$ system. They nucleate gas hydrates on cooling; however, no further heterogenization ($F \rightarrow L + V$) in the non-aqueous part of the inclusion has been observed. Therefore, no molar volume calculations can be done since T_h data are not available.

Type III inclusions can be plotted within the $\text{CH}_4\text{-N}_2$ system taking $X\text{N}_2 + X\text{CH}_4 = 1$, because it is assumed that all CO_2 is partitioned in the solid phase at T_h $\text{CH}_4 + \text{N}_2$. Molar volume calculations have been made in the VT diagram for $\text{CH}_4\text{-N}_2$ (van den Kerkhof, 1988b), with a correction for solid CO_2 (\bar{V} solid $\text{CO}_2 = 28.2 \text{ cm}^3 \cdot \text{mol}^{-1}$). For inclusions with homogenization into the liquid, the molar volume is about $63 \text{ cm}^3 \cdot \text{mol}^{-1}$ and density around $0.44 \text{ g} \cdot \text{cm}^{-3}$. With homogenization into the vapour phase more abundant, it is not possible to calculate the molar volume accurately. However, if homogenization into the vapour phase is near critical, the molar volume can be approximated as $77 \text{ cm}^3 \cdot \text{mol}^{-1}$ (\bar{V} for critical region, with CO_2 correction, van den Kerkhof, 1988b) and therefore, the density is about $0.37 \text{ g} \cdot \text{cm}^{-3}$. It can be concluded that type III fluid is a low-density fluid, with density less than $0.42 \text{ g} \cdot \text{cm}^{-3}$.

Type IV inclusions belong to the $\text{N}_2\text{-CH}_4$ system, but the absence of relevant T_h $\text{CH}_4\text{-N}_2$ data makes it impossible to calculate the molar volume of their nonaqueous part. Given the difficulty of such calculations for type I, II and IV inclusions, their bulk molar volume and bulk compositions cannot be obtained.

Fluid evolution and genetic model

The composition of all four fluid inclusion types are presented on a ternary $\text{N}_2\text{-CH}_4\text{-CO}_2$ (Fig. 5). Even if the lack of data on bulk composition poses a problem, the evolution of the non-aqueous part of inclusions can be obtained from this diagram. In the studied quartz samples, gas compositions in fluid inclusions are always characterized by CH_4 , CO_2 and N_2 mixtures, from CO_2 -rich mixtures in the earliest inclusions (type I) to N_2 -rich mixtures in the latest inclusions (type IV). The temperature of total homogenization decreases in the same direction. Hence, a progressive cooling of the fluid is correlated with an N_2 enrichment of its non-aqueous part.

The lack of water in the type III fluid could bring into question whether these inclusions belong to the same evolution line of I, II and IV

aqueous-rich inclusions. Microscopic textural observations support the contemporaneity between type II and III inclusions and the coexistence of these fluids of contrasted physical features, notably density, suggests an immiscibility phenomenon at the time of trapping.

The immiscibility or boiling is described as the coexistence of two phases of a given composition in equilibrium along the solvus surface of the system defined by the previously homogeneous fluid (Pichavant *et al.*, 1982; Touret, 1987). Derived from this definition the boiling criteria (Ramboz *et al.*, 1982; Touret, 1987) are well delimited, and severely constraint the interpretation of the fluid-inclusion data in terms of immiscibility.

Since some contemporaneous relationships between type II and type III inclusions may be observed, these two types of inclusions could represent liquid-rich and gaseous-rich unmixed fluids respectively. Both types of fluid inclusion are well represented in the same samples and they often appear in the same regions of the sample. They also sometimes occur in well separated domains: type II occur in clusters, while type III occur in trails. These different distributions do not pose a problem regarding coexistence, since boiling results in a sudden expansion of part of the fluid (in this case to the low-density type III fluid) and intense fracturing of the rock (Touret, 1987). Hence, the vapour-rich inclusions are distributed in arrangements reflecting the great expansion of their molar volume, and the liquid-rich, less mobile inclusions, remain in groups.

The two types of inclusion resulting from an unmixing must homogenize in the same temperature range, one type into the liquid and the other into the vapour; if one inclusion type decrepitates before homogenization, the other type must behave similarly. The type II inclusions homogenize into liquid between 190 and 330 °C, and show decrepitation before homogenization between 230 and 310 °C. However, the type III inclusions are water-free or, at least, the water volume is less than 10%, the limit of detection by optical microscopy. Therefore, T_H data are unattainable from them and it is not possible to verify whether this immiscibility condition is reached in this case study.

Regarding the PT trapping conditions, in an immiscibility phenomena they are fixed and correspond to PT at homogenization. In the fluid type II the decrepitation of the inclusions before homogenization determine a P of about 0.9–1 kbar (Leroy, 1979). Although this decrepitation prevents a well defined peak in the T_H histogram, the trapping temperature can be

estimated at about 275–300 °C. Note that since decrepitation occur before homogenization is achieved, the T_H for these inclusions must be higher than their T_D . Isochores calculated for a representative type III inclusion assuming 5% (volume) of water (see appendix) give pressures of 920 bars for $T = 300$ °C, which is consistent with the PT conditions obtained from the types II inclusions.

An important point is to determine whether the unmixing of a given homogeneous fluid can give rise to a type III fluid with less than 10% of water (in volume) coexisting in equilibrium with the fluid II at the described PTX immiscibility conditions. In other words, type II and type III inclusions must fit with the immiscibility surface of the relevant system.

Experimental data on the solvus surface for the complex $H_2O-CO_2-CH_4-N_2$ system are not available. However, a brief estimation can be made with the H_2O-CH_4 (Welch, 1973) and H_2O-N_2 binary systems (Japas and Franck, 1985) which are, among the available experimental systems, the closest to the fluid composition of interest. In the PX projection of the two-phase region (Fig. 6a, b) the 1 kbar isobar, crossing the 300 °C isotherms, give two compositions in each diagram: 80 mol% and 5 mol% CH_4 (Fig. 6a) and N_2 (Fig. 6b) respectively. The bulk composition

of the type III inclusions (calculated containing less than 10% vol of water, see appendix) and type II respectively are largely consistent with these values. Therefore, it is possible that type II and III inclusions are the two immiscible parts of a previously homogeneous fluid.

Conclusion

The immiscibility phenomenon, in this case, cannot be clearly demonstrated, since several approximations are needed in the interpretation of the data. However, it is clear that there is some good evidence, and the occurrence of immiscibility is a plausible hypothesis.

Precipitation of gold and minor sulphides in V2 veins can be related to type I CO_2 -rich fluid inclusions at temperatures in the region of 380 °C. These inclusions and native gold occur only in V2 veins.

A subsequent drop in XCO_2 and cooling are recorded in type II and III inclusions, the unmixed parts of a previously homogeneous fluid which boiled at 300 °C and 1 kbar due to sudden drops of P in dilational jogs (V3 veins). In this unmixing, the more volatile compounds are partitioned in favour of the vapour phase and, hence type III inclusions are richer in N_2 and CH_4 than type II, which concentrates mainly H_2O ,

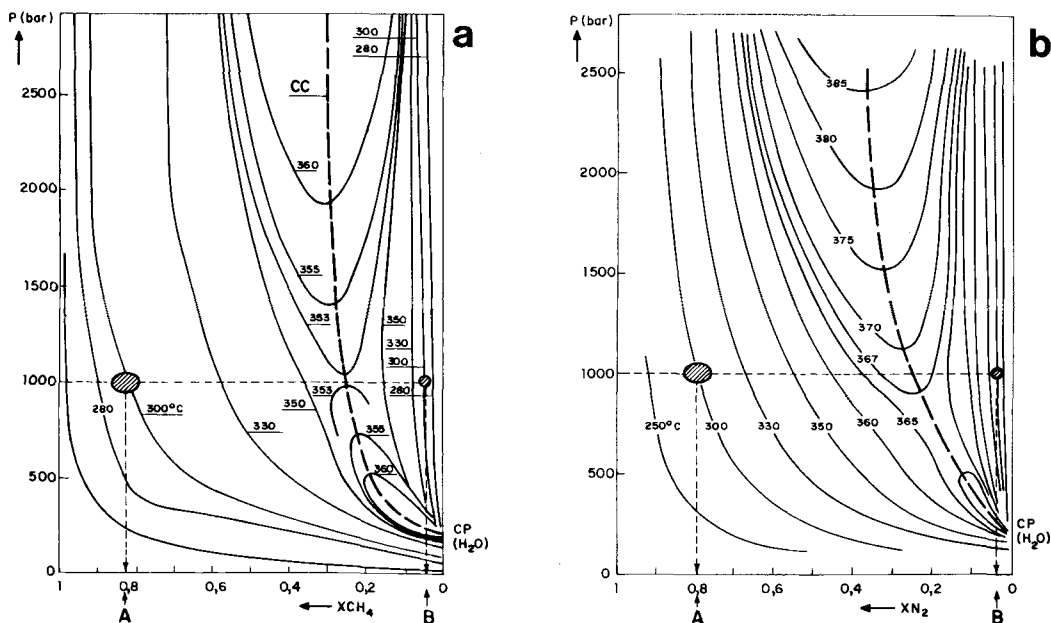


Fig. 6 (a, b). P - T - X diagram for the H_2O-CH_4 (Welch, 1973) and H_2O-N_2 (Japas and Franck, 1985) systems. CC = critical curve. CP (H_2O) \approx critical point for pure water. A and B: Compositional values given by the 1 kbar isobar intersecting 300 °C isotherms. These compositions are consistent with type III and type II inclusions respectively.

higher CO₂ and probably salts. This boiling produced the precipitation of the stibnite, which is the main mineralizing event in the Mari Rosa deposit.

The type IV inclusions, the richest in H₂O, were probably derived from type II fluid and represent a late fluid circulation, volumetrically less important and at lower temperatures (T_H between +190 to +275 °C). This was the final stage in the evolution of the fluid phase with a total loss of CO₂ and maximum enrichment in N₂.

In the absence of isotope and organic geochemical data, the origin of the fluid is difficult to ascertain. However, the observed abundance of carbonaceous matter in the host rocks, notably in the black shales, points to a biogenic origin for nitrogen and carbon. During diagenesis and low-grade metamorphism of organic-bearing sediments, nitrogen is stored as NH₄⁺ in clay minerals while carbon is retained as amorphous carbon compounds. This origin has been reported for N₂ in a number of metamorphic and geothermal environments (Honma and Itihara, 1981; Kreulen and Schuiling, 1982; Duit *et al.*, 1986; Dubessy and Ramboz, 1986; Darimont *et al.*, 1988; Bottrell *et al.*, 1988; Dubessy *et al.*, 1989). However, even if the black shales could be the source of these elements, the chloritic alteration in the wall-rocks adjacent to the earlier mineralized veins (V2) and argillic in the later (V3) indicate that the fluid was not in equilibrium with the host rocks. This leads to the conclusion that the original fluid was not necessarily a metamorphic fluid derived from these rocks but an external fluid introduced into them.

The CO₂ present in the early fluid could be either a primary characteristic of the initial incoming fluid or the result of a fluid-rock interaction between host rock and fluid of the type:



However, the progressive enrichment in N₂ recorded in Mari Rosa fluid inclusions suggest that consumption of CO₂ by the reaction (postulated by Kreulen and Schuiling, 1982)



progressed to the point of total loss of CO₂ by the fluid during its evolution.

Acknowledgements

The authors are indebted to J. L. R. Tourret for fruitful discussions and to A. M. van den Kerckhof and C. Ramboz for their helpful suggestions and interest. We also thank R. Oyarzun for the review of the English text.

References

- Bottrell, S. H., Shepherd, T. J., Yardley, B. W. D., and Dubessy, J. (1988) A fluid inclusion model for the genesis of the ores of the Dolgellau Gold Belt, North Wales. *J. Geol. Soc. London*, **145**, 139–45.
- Bozzo, A. T., Chen, H. S., Kass, J. R., and Barduhn, A. J. (1975) The properties of the hydrates of chlorine and carbon dioxide. *Desalination*, **16**, 303–20.
- Burrus, R. C. (1981) Analysis of phase equilibria in C–O–H–N–S fluid inclusions. *Mineral. Assoc. Canada Short Course Handbook*, **6**, 39–74.
- Chen, H. S. (1972) *The thermodynamics and composition of carbon dioxide hydrate*. Unpub. M.Sc. thesis. Syracuse Univ., 67 pp.
- Collins, P. L. F. (1979) Gas hydrates in CO₂-bearing fluid inclusions and the use of freezing data for estimation of salinity. *Econ. Geol.*, **74**, 1435–44.
- Darimont, A., Burke, T., and Tourret, J. (1988) Nitrogen-rich metamorphic fluids in devonian meta-sediments from Bastogne, Belgium. *Bull. Min.*, **111**, 321–30.
- Dhamelincourt, P., Beny, J. M., Dubessy, J., and Poty, B. (1979) Analyse d'inclusions fluides à la microsonde MOLE à effet Raman. *Ibid.*, **107**, 600–10.
- Dubessy, J. (1984) Simulation des équilibres chimiques dans le système C–O–H. Conséquences méthodologiques pour les inclusions fluides. *Ibid.*, **107**, 155–68.
- and Ramboz, C. (1986) The history of organic nitrogen from early diagenesis to amphibolite facies: mineralogical, chemical, mechanical and isotopic implications. *5th Int. Symp. Water-Rock Interaction*. Reykjavik, Iceland, August 8–17. Extended Abstracts, 170–4.
- Poty, B., and Ramboz, C. (1989) Advances in C–O–H–N–S fluid geochemistry based on micro-Raman spectrometric analysis of fluid inclusions. *Eur. J. Mineral.*, **1**, 517–34.
- Duit, W., Jansen, J. B. H., Van Breenen, A., and Bos, A. (1986) Ammonium micas in pelitic rocks as exemplified by Dôme de l'Agout (France). *Am. J. Sci.*, **286**, 702–22.
- Gumiel, P. (1983) Metalogenia de los yacimientos de Sb de la Península Ibérica. *Tecniterae*, **2**, 6–120.
- and Arribas, A. (1987) Antimony deposits in the Iberian Peninsula. *Econ. Geol.*, **82**, 1453–63.
- and Saavedra, J. (1976) Geología y metalogenia del yacimiento de estibina-scheelita de San Antonio, Alburquerque (Badajoz). *Studia Geol.*, **10**, 61–93.
- Hand, J. H., Katz, D. L., and Verma, V. K. (1974) Review of gas hydrates with implication for ocean sediments. In *Natural Gases in Marine Sediments* (I. Kaplan, ed.). Plenum Press, 179–94.
- Hanor, J. S. (1980) Dissolved methane in sedimentary brines: Potential effect on the PVT properties of fluid inclusions. *Econ. Geol.*, **75**, 603–17.
- Hollister, L. S. and Burrus, R. C. (1976) Phase equilibria in fluid inclusions from the Khtada Lake metamorphic complex. *Geochim. Cosmochim. Acta*, **40**, 163–75.

- Holloway, J. R. (1981) Compositions and volumes of supercritical fluids in the earth's crust. *Min. Assoc. Canada Short Courses Handbook*, 6, 13–38.
- Honma, H. and Itihara, Y. (1981) Distribution of ammonia in minerals of metamorphic and granitic rocks. *Geochim. Cosmochim. Acta*, 45, 983–8.
- Japas, M. L. and Franck, E. U. (1985) High-pressure phase equilibria and PVT data of the water–nitrogen system to 673 K and 250 MPa. *Ber. Bunsenges. Phys. Chem.*, 89, 793–800.
- Kerkhof, A. M. van den (1988a) Phase transition and molar volumes of CO₂–CH₄–N₂ inclusions. *Bull. Min.*, 111, 257–66.
- (1988b) *The system CO₂–CH₄–N₂ in fluid inclusions: theoretical modelling and geological applications*. Ph.D. Thesis. Free University Press, Amsterdam, 206 pp.
- Kreulen, R. and Schuiling, R. D. (1982) N₂–CH₄–CO₂ fluids during formation of the Dôme de l'Agout, France. *Geochim. Cosmochim. Acta*, 46, 193–203.
- Leroy, J. (1979) Contribution a l'etalonnage de la pression interne des inclusions fluides lors de leur décrepitation. *Bull. Mineral*, 102, 584–93.
- Martín Herrero, D. and Bascones, L. (1979) Memoria explicativa de la Hoja 674, Sever-Santiago de Alcántara (MAGNA). *Inst. Geol. Minero España*, 25 pp.
- Parrish, W. R. and Prausnitz, J. M. (1972) Dissociation pressures of gas hydrates formed by gas mixtures. *Ind. Eng. Chem. Process. Des. Develop.*, 11, 26–35.
- Pichavant, M., Ramboz, C., and Weibrod, A. (1982) Fluid immiscibility in natural processes: use and misuse of fluid-inclusion data. I. Phase equilibria analysis. A theoretical and geometrical approach. *Chem. Geol.*, 37, 1–27.
- Poty, B., Leroy, J., and Jachimowicz, L. (1976) Un nouvel appareil pour la mesure des températures sous le microscope: l'installation de microthermométrie Chaixmecca. *Bull. Soc. Fr. Minéral. Cristallogr.*, 99, 182–6.
- Quesada, C., Florido, P., Gumiel, P., and Osborne, J. (1987) Memoria Explicativa del Mapa Geológico y Minero de Extremadura. Junta de Extremadura, 126 pp.
- Ramboz, C., Pichavant, M., and Weisbrod, A. (1982) Fluid immiscibility in natural processes: use and misuse of fluid inclusion data. II. Interpretation of fluid inclusion data in terms of immiscibility. *Chem. Geol.*, 37, 29–48.
- Schnapper, D., and Dubessy, J. (1985) The P–V–T–X–f_{O₂} evolution of H₂O–CO₂–CH₄-bearing fluid in a wolframite vein: Reconstruction from fluid inclusion studies. *Geochim. Cosmochim. Acta*, 49, 205–19.
- Roedder, E. (1976) Fluid inclusion evidence on the genesis of ores in sedimentary and volcanic rocks. *Handbook of stratabound and stratiform ore deposits*, 4 (K. H. Wolf, ed.), Elsevier Sc. Pub. Co. Amsterdam.
- (1984) Fluid inclusions. *Reviews in Mineralogy*, 12, 644 pp. Mineral. Soc. Am.
- Seitz, J. C., Pasteris, J. D., and Wopenka, B. (1987) Characterization of CO₂–CH₄–H₂ fluid inclusions by microthermometry and laser Raman microprobe spectroscopy: Inferences from clathrate and fluid equilibria. *Geochim. Cosmochim. Acta*, 51, 1651–64.
- Stone, H. W. (1943) Solubility of water in liquid carbon dioxide. *Indus. Eng. Chem.*, 35, 1284–6.
- Swanenberg, H. E. C. (1979) Phase equilibria in carbonic systems and their application to freezing studies of fluid inclusions. *Contrib. Mineral. Petrol.*, 68, 303–6.
- (1980) Fluid inclusions in high-grade metamorphic rocks from S.W. Norway. *Geologica Utraiectina*, 25, (Univ. Utrecht), 146 pp.
- Touray, J. C., Beny, C., Dubessy, J., and Guilhaumou, N. (1985) Microcharacterization of fluid inclusions in minerals by Raman microprobe. *Scanning Electron microscopy*, 1, 103–18.
- Touret, J. (1987) Fluid inclusions and pressure–temperature estimates in deep-seated rocks. *Chemical Transport in Metasomatic Processes* (H. C. Helgeson, ed.), D. Riedel Publ. Co., 91–121.
- Unruh, C. H. and Katz, D. L. (1949) Gas hydrates of carbon dioxide–methane mixtures. *Petrol. Trans. AIME*, 186, 83.
- Welch, H. (1973) *Die systeme xenon–wasser und methan–wasser bei hohen drücken und temperaturen*. Ph.D. thesis. Institute for Physical Chemistry, Karlsruhe.

[Manuscript received 6 July 1989;
revised 27 July 1990]

Appendix

Calculations of the bulk composition, bulk density and isochores for a type III inclusion, assuming 0% and 5% (volume) of H₂O (method from Ramboz *et al.*, 1985).

$$n\text{H}_2\text{O} = \frac{(1 - \text{Df})d}{18}$$

$$n\text{CO}_2 = \frac{\text{Df.dv.ZCO}_2}{44 - 16\text{ZCH}_4 - 28\text{N}_2}$$

$$n\text{CH}_4 = \frac{\text{Df.dv.ZCH}_4}{44 - 16\text{ZCH}_4 - 28\text{N}_2}$$

$$n\text{N}_2 = \frac{\text{Df.dv.ZN}_2}{44 - 16\text{ZCH}_4 - 28\text{N}_2}$$

$$X_i = \frac{n_i}{n\text{H}_2\text{O} + n\text{CO}_2 + n\text{CH}_4 + n\text{N}_2}$$

$$d = (1 - \text{Df}) + \text{Df.dv}$$

$$\bar{V} = \frac{\sum x_i \cdot \text{Mwt}_i}{d}$$

0% H₂O (Df = 1)

$$X\text{CO}_2 = 0.21$$

$$X\text{CH}_4 = 0.18$$

$$X\text{N}_2 = 0.61$$

$$d = 0.37 \text{ g.cm}^{-3}$$

$$\bar{V} = 78 \text{ cm}^3 \cdot \text{mol}^{-1}$$

5% H₂O (Df = 0.95)

$$X_{\text{H}_2\text{O}} = 0.16$$

$$X_{\text{CO}_2} = 0.17$$

$$X_{\text{CH}_4} = 0.15$$

$$X_{\text{N}_2} = 0.52$$

$$d = 0.4 \text{ g} \cdot \text{cm}^{-3}$$

$$\bar{V} = 68 \text{ cm}^3 \cdot \text{mol}^{-1}$$

Isochore: 275 °C 857 bars
 300 °C 922 bars

The isochore was calculated with the Amsterdam-Oslo fluid program, based on Holloway program (Holloway, 1981).

Calculation of the bulk composition for a type II fluid inclusion, assuming $dv = 0.37 \text{ g} \cdot \text{cm}^{-3}$

Since a dv calculation cannot be done in type II inclusions, the bulk composition is approximated for a density $dv = 0.37 \text{ g} \cdot \text{cm}^{-3}$ (density considered for type III inclusion used in the above calculation).

$$Df = 0.15$$

$$Z_{\text{CO}_2} = 0.4$$

$$Z_{\text{CH}_4} = 0.1$$

$$Z_{\text{N}_2} = 0.5$$

$$X_{\text{H}_2\text{O}} = 0.96$$

$$X_{\text{CO}_2} = 0.016$$

$$X_{\text{CH}_4} = 0.004$$

$$X_{\text{N}_2} = 0.02$$

$$dv = 0.37 \text{ g} \cdot \text{cm}^{-3}$$

$$dv = 0.9 \text{ g} \cdot \text{cm}^{-3}$$

$$\bar{V} = 20 \text{ cm}^3 \cdot \text{mol}^{-1}$$